Supporting Information

Tuning Quantum Tunnelling of Magnetization through 3d-4f Magnetic Interaction: the Alternative Approach for Manipulating Single-molecule Magnetism

Jing Li,[a] Rong-Min Wei,[a] Tian-Cheng Pu,[c] Fan Cao,[a] Li Yang,[a] Yuan Han,[a] Yi-Quan Zhang,*[b] Jing-Lin Zuo,*[a] and You Song*[a]

Table S1. Crystallographic data for complexes **1-3**.

	1	**2**	**3**
Formula	$C_{62}H_{60}Dy_2N_6O_{20}Zn_2$	$C_{66}H_{66}Dy_2Mn_2N_8O_{20}$	$C_{78}H_{94}Co_2Dy_2N_{12}O_{24}$
*M*r[gmol^{-1}]	1664.90	1726.15	2026.51
Crystal system	Triclinic	Monoclinic	Triclinic
Space group	$P\bar{1}$	$P2_1/c$	$P\bar{1}$
a[Å]	11.4697(13)	10.970(2)	11.8868(11)
b[Å]	11.6701(14)	16.084(3)	11.8963(11)
c[Å]	13.4425(16)	20.340(3)	14.6976(13)
α[°]	86.002(2)	90.00	90.589(2)
β[°]	66.152(2)	114.546(7)	94.010(2)
γ[°]	68.286(2)	90.00	98.338(3)
V[Å^{-3}]	1522.1(3)	3264. 5(10)	2050.9(3)
T[K]	296(2)	296(2)	173(2)
Z	1	2	1
ρ_{calcd} /g cm^{-3}	1.816	1.756	1.641
data measured	10244	21390	7136
indep reflns	6969	7530	7136
R_{int}	0.0224	0.0353	-- (non-merohedral twin)
reflnswith I>2s(*I*)	5565	5740	5578
parameter	421	446	541
restraints	0	21	0
*R*1,*wR*2	0.0364, 0.0892	0.0383,0.0901	0.0527, 0.1105
GOF	1.019	1.053	1.186
Largest residuals [e Å^{-3}]	1.452, -0.985	0.959,-0.807	1.093, -1.972

$R1=\Sigma||F_0|-|F_c||/\Sigma|F_0|$, $wR2=\{\Sigma[w(F_0^2-F_c^2)^2]/\Sigma[w(F_0^2)^2]\}^{1/2}$

Table S2. Selected distance [Å] and angles [°] for **1-3**.

	1 (Zn_2 Dy_2)[a]	**2** (Mn_2 Dy_2)[b]	**3** (Co_2 Dy_2)[c]
M1-O1	2.068(3)	2.135(3)	2.131(7)
M1-O4	2.071(3)	2.161(3)	2.074(7)
M1-O5	2.065(3)	2.127(3)	2.028(7)
M1-N2	2.053(4)	2.147(3)	2.079(9)
M1-O1^{i}	2.301(3)	2.467(3)	2.219(7)
Dy1-O1	2.393(3)	2.366(3)	2.386(7)
Dy1-N1	2.450(4)	2.456(4)	2.474(8)
Dy1-O2	2.153(3)	2.167(3)	2.156(7)
Dy1-O5	2.299(3)	2.316(3)	2.305(6)
Dy1-O6	2.520(3)	2.487(3)	2.509(7)
Dy1-O4	2.316(4)	2.321(3)	2.330(7)
Dy1-O7	2.488(5)	2.451(4)	2.463(9)
Dy1-O8	2.478(4)	2.484(4)	2.477(8)
Dy1-Dy1^{i}	6.196(3)	6.292(4)	6.163(7)
O2-Dy1-N1	75.7(3)	74.8(6)	75.7(3)
O2-Dy1-O6	83.9(6)	83.2(5)	83.7(2)
O6-Dy1-O5	64.6(1)	64.9(9)	64.1(2)
O5-Dy1-O1	69.0(5)	69.8(6)	69.2(2)
O1-Dy1-N1	68.4(2)	68.5(6)	67.5(2)
O6-Dy1-O4^{i}	88.1(2)	86.8(8)	86.8(2)
O1-M1-O5	80.1(4)	77.9(5)	79.7(3)
O1-M1-O1^{i}	83.0(1)	83.8(8)	82.7(3)
O1-M1-O10	89.3(1)	98.5(9)	88.2(3)
O1-M1-O4	111.0(6)	116.9(7)	111.3(3)
O5-M1-N2	87.9(2)	85.1(9)	89.5(3)

Symmetry code: (a) i, −x, −y, −z; (b) x, y, z ; -x+1/2, y+1/2, -z+1/2; -x, -y, -z; x-1/2, -y-1/2, z-1/2; (c) i, −x, −y, −z.

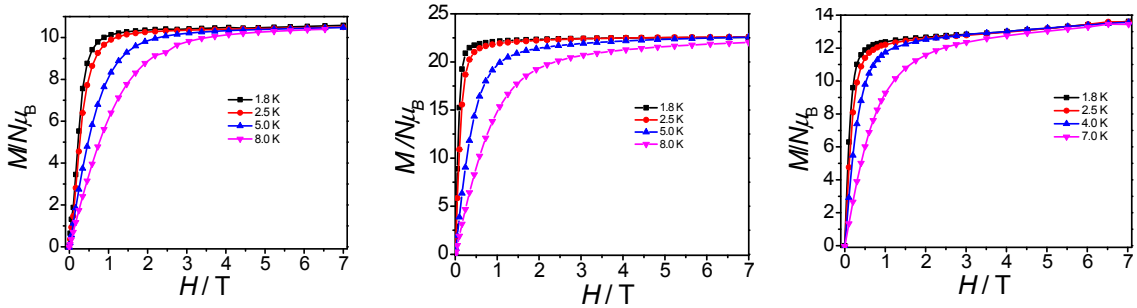

Fig. S1 . Field dependence of the magnetization, *M*, at different temperature for complex **1** (left) **2** (middle) and **3** (right).

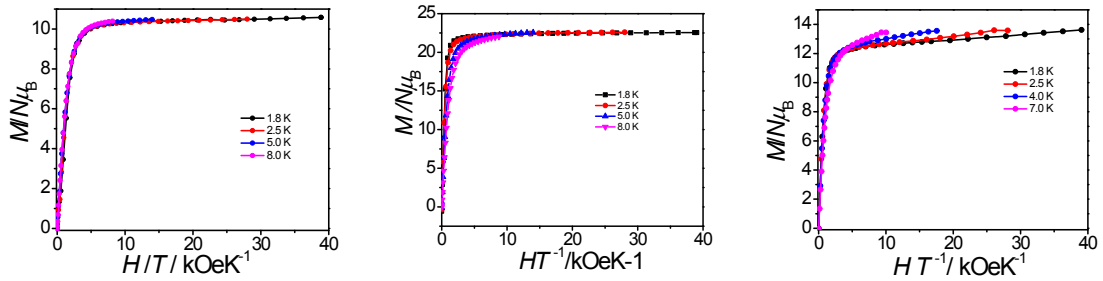

Fig. S2. Experimental *M* vs. *H*/*T* plots at different temperatures for complex **1** (left), **2** (middle) and **3** (right).

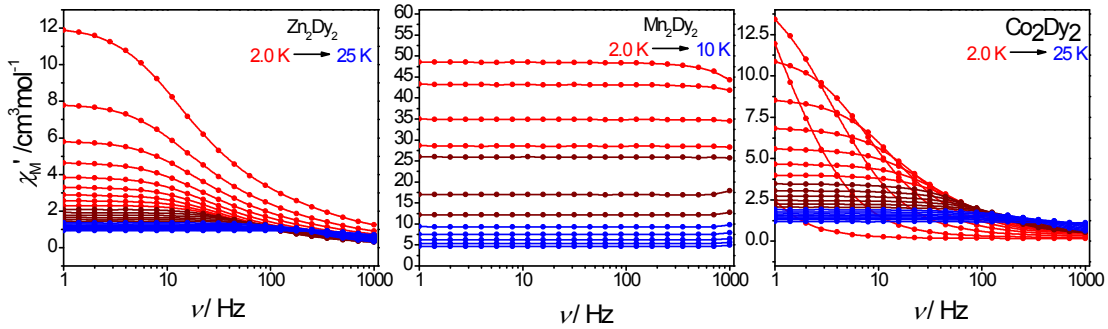

Fig. S3. Frequency dependence of in-phase (χ_M') ac susceptibilities under zero dc field (1-999 Hz, by MPMS Squid VSM) at indicated temperatures for complex **1** (left), complex **2** (middle) and complex **3** (right).

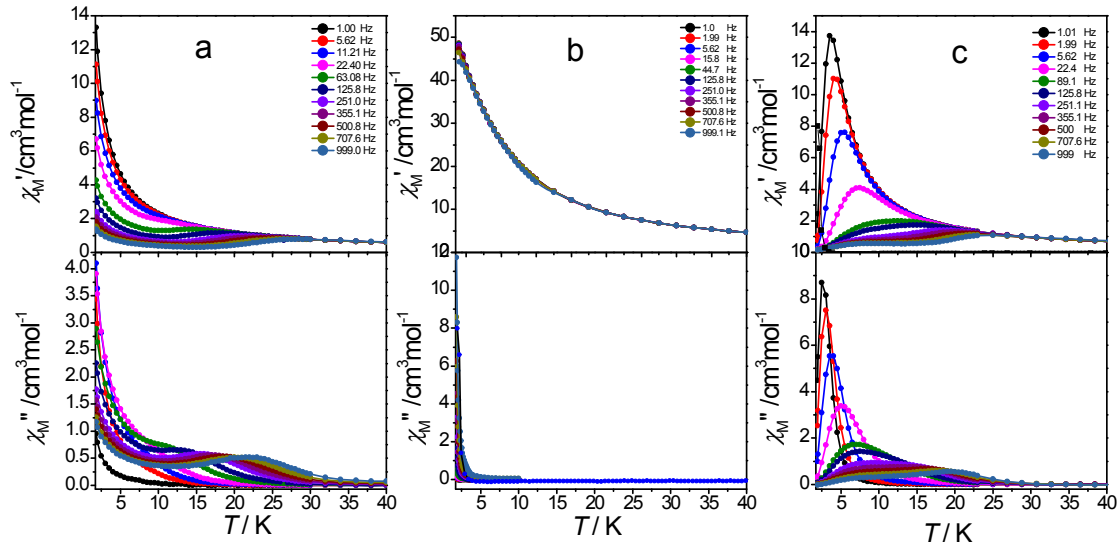

Fig. S4. Temperature dependence of in-phase (χ_M') and out-of- phase (χ_M'') ac susceptibilities under zero dc field (1-999 Hz, by MPMS Squid VSM) at indicated temperatures for complexes **1** (a), **2** (b) and **3** (c).

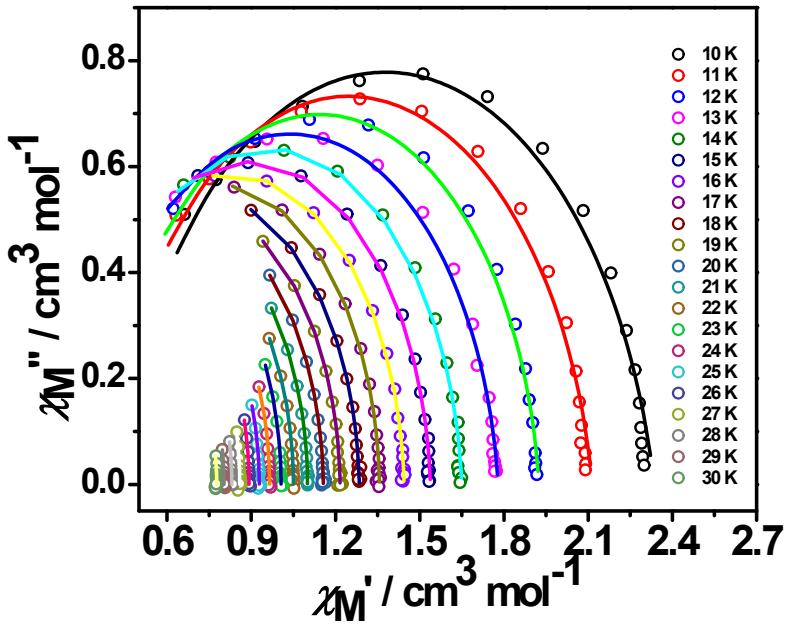

Fig. S5. Variable temperature Cole-Cole plots of complex **1** under zero dc field (1-999 Hz, by MPMS Squid VSM). Fitted parameters are compiled in supplementary Table S3.

Table S3. Analysis of Cole-Cole plot of complex **1** under zero dc field.

T	χ_S	χ_t	τ	α	R
10 K	0.233452E+01	0.420764	0.913310E-02	0.130631	0.203476E-01
11 K	0.211440E+01	0.380732	0.111223E-01	0.107042	0.128025E-01
12 K	0.192439E+01	0.363200	0.137557E-01	0.709362E-01	0.381246E-01
13 K	0.177897E+01	0.299583	0.176124E-01	0.709294E-01	0.353606E-02
14 K	0.164978E+01	0.274980	0.221716E-01	0.512202E-01	0.194491E-02
15 K	0.153771E+01	0.242014	0.281728E-01	0.390024E-01	0.984554E-03
16 K	0.144427E+01	0.210597	0.355637E-01	0.324423E-01	0.576597E-03
17 K	0.135643E+01	0.188500	0.444942E-01	0.193296E-01	0.492120E-03
18 K	0.128454E+01	0.142592	0.569744E-01	0.238841E-01	0.410988E-03
19 K	0.121621E+01	0.123942	0.705093E-01	0.170176E-01	0.375996E-03
20 K	0.115624E+01	0.103249	0.870767E-01	0.127869E-01	0.279320E-03
21 K	0.110032E+01	0.817343	0.106785	0.666913E-02	0.116946E-03
22 K	0.104986E+01	0.519696E-01	0.132329	0.377118E-02	0.269313E-03
23 K	0.100585E+01	0.215072E-01	0.164662	0.310139E-02	0.218729E-03
24 K	0.965114	0.387684E-14	0.202509	0.499554E-02	0.218781E-03
25 K	0.928476	0.456334E-14	0.244837	0.685372E-02	0.261986E-03
26 K	0.891963	0.255670E-14	0.288075	0.641754E-15	0.121588E-03
27 K	0.858794	0.329153E-14	0.342789	0.872076E-15	0.390097E-03
28 K	0.830292	0.449946E-14	0.408077	0.649119E-15	0.239435E-03
29 K	0.802523	0.572966E-14	0.486920	0.766481E-15	0.173047E-03
30 K	0.776499	0.768307E-14	0.575190	0.100719E-14	0.277453E-03

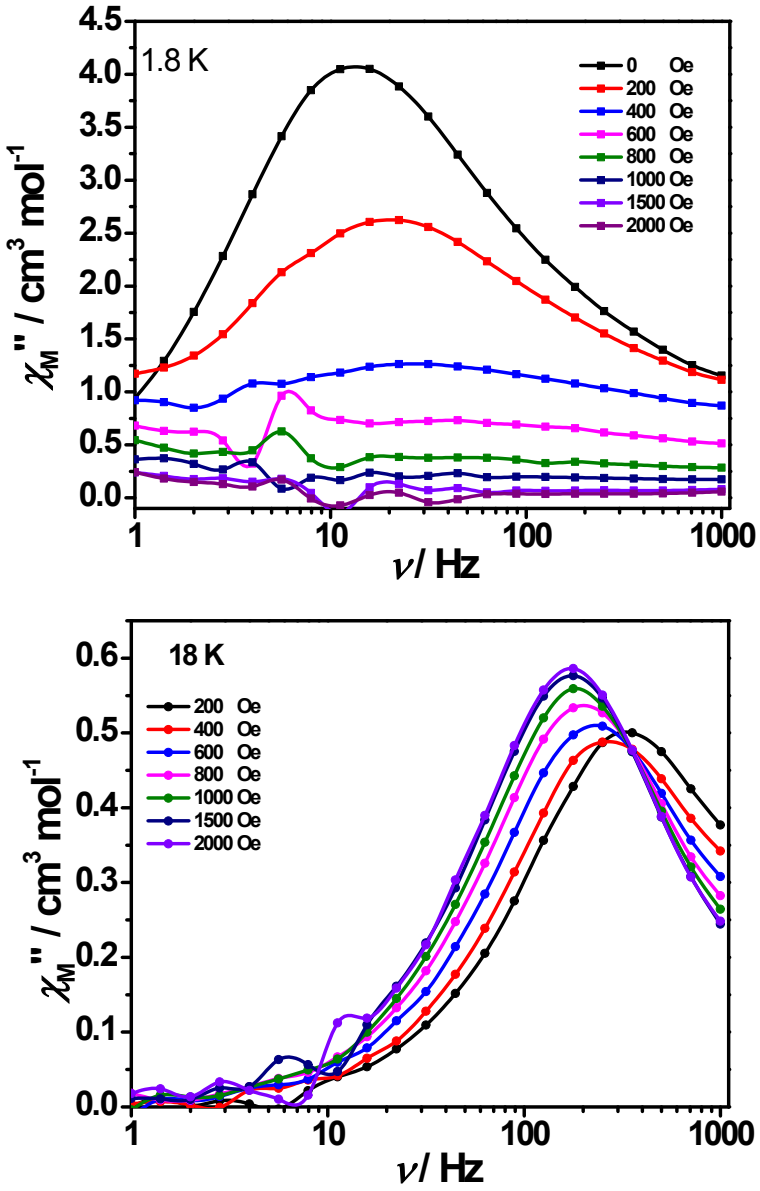

Fig. S6. Variable-frequency out-of-phase χ_M" components of the ac magnetic susceptibility collected for a microcrystalline sample of **1** (up, at 1.8 K; down, at 18 K) under different applied dc fields.

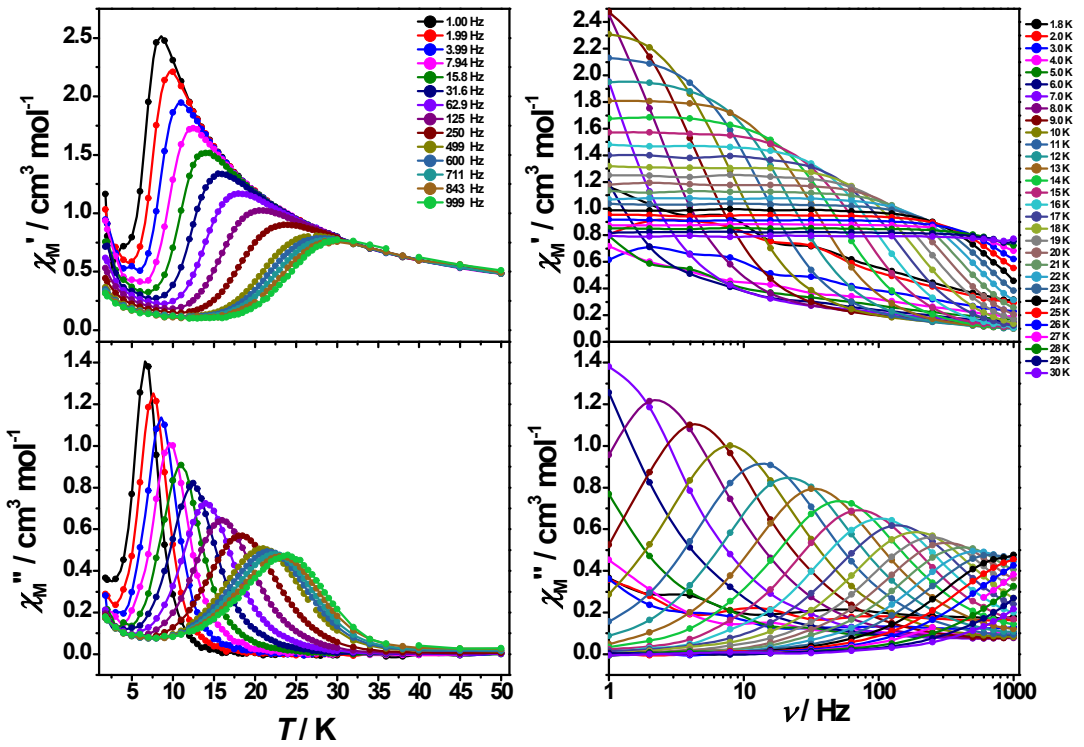

Fig. S7. Temperature (left) and frequency (right) dependence of in-phase (χ_M') and out-of- phase (χ_M") ac susceptibilities applied 1000 Oe dc field (1-999 Hz, by MPMS Squid VSM) at indicated temperatures for complex **1**.

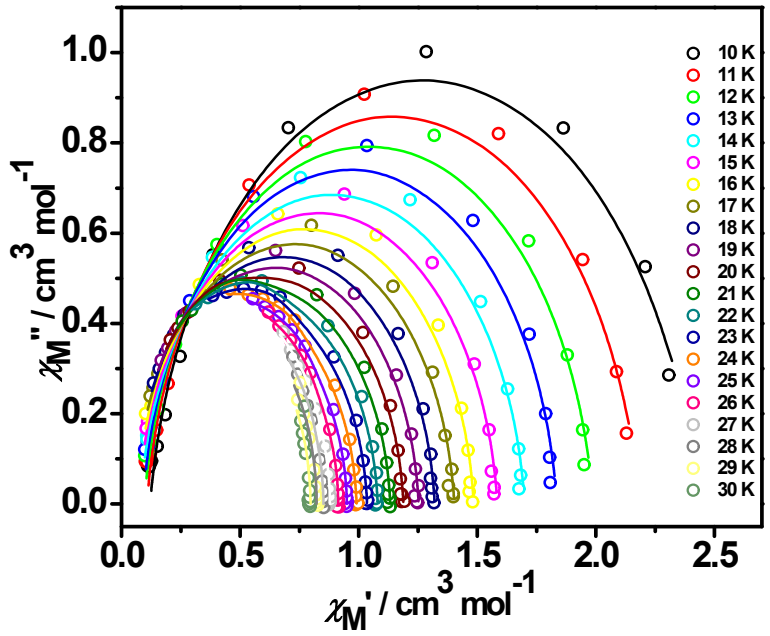

Fig. S8. Variable temperature Cole-Cole plots of complex **1** in the dc field of 1000 Oe (1-999 Hz, by MPMS Squid VSM). Fitted parameters are compiled in supplementary Table S4.

Table S4. Analysis of Cole-Cole plot of complex **1** under 1000 Oe dc field.

T	χ_S	χ_t	τ	α	R
10 K	0.120528	0.241688E+01	0.193704E-01	0.956568E-01	0.173544E-01
11 K	0.106855	0.217930E+01	0.113254E-01	0.859617E-01	0.131947E-01
12 K	0.967975E-01	0.198686E+01	0.693561E-02	0.768687E-01	0.109759E-01
13 K	0.909207E-01	0.183443E+01	0.446914E-02	0.680684E-01	0.888834E-02
14 K	0.802680E-01	0.169943E+01	0.300215E-02	0.706548E-01	0.617078E-02
15 K	0.721284E-01	0.158414E+01	0.207945E-02	0.650753E-01	0.526768E-02
16 K	0.644832E-01	0.148507E+01	0.148462E-02	0.613962E-01	0.422791E-02
17 K	0.543530E-01	0.140291E+01	0.109001E-02	0.642485E-01	0.297800E-02
18 K	0.516186E-01	0.132024E+01	0.812476E-03	0.565906E-01	0.178009E-02
19 K	0.468300E-01	0.125243E+01	0.616307E-03	0.528309E-01	0.182974E-02
20 K	0.384377E-01	0.118835E+01	0.473033E-03	0.508631E-01	0.156753E-02
21 K	0.294567E-01	0.113287E+01	0.367256E-03	0.494545E-01	0.130743E-02
22 K	0.193949E-01	0.108004E+01	0.286247E-03	0.451786E-01	0.113447E-02
23 K	0.841788E-02	0.103539E+01	0.225103E-03	0.452799E-01	0.643144E-03
24 K	0.689153E-15	0.991049	0.176780E-03	0.375115E-01	0.777436E-03
25 K	0.955277E-15	0.950470	0.140089E-03	0.291330E-01	0.917246E-03
26 K	0.120055E-14	0.914037	0.112896E-03	0.184911E-01	0.680183E-03
27 K	0.226604E-14	0.878224	0.895351E-04	0.391397E-14	0.108619E-02
28 K	0.322103E-14	0.850987	0.725229E-04	0.508117E-14	0.756533E-03
29 K	0.411508E-14	0.823027	0.575238E-04	0.673320E-14	0.102428E-02
30 K	0.610333E-14	0.796939	0.448247E-04	0.613247E-14	0.162437E-02

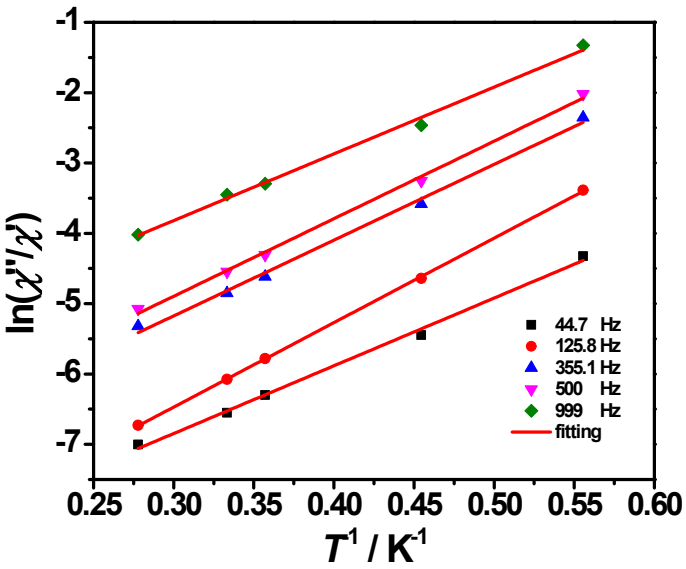

Fig. S9. (Color online) Natural logarithm of the ratio of χ'' over χ' versus T^{-1} of the data for complex **2** given in Fig. S4b slope corresponding to activation energy E_a = 11 K.

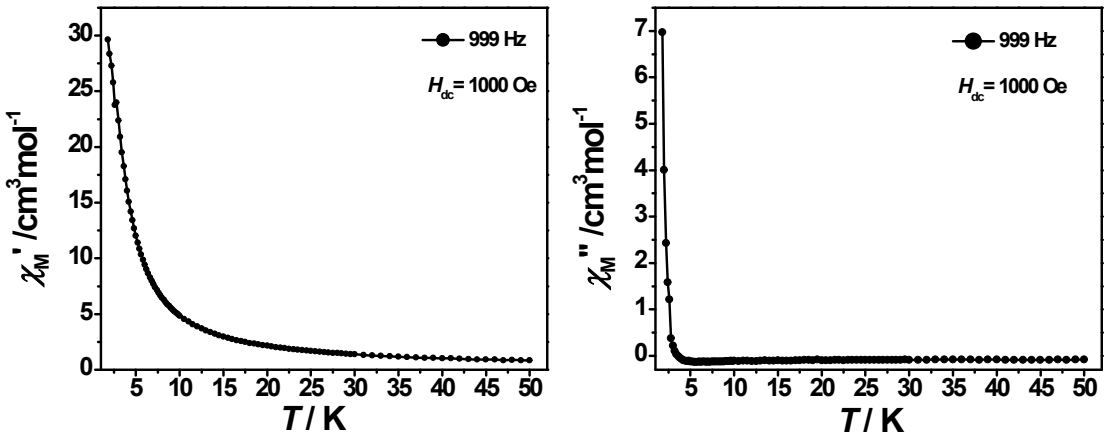

Fig. S10. Temperature dependence of in-phase (χ_M') and out-of- phase (χ_M'') ac susceptibilities applied 1000 Oe dc field (999 Hz, by MPMS Squid VSM) at indicated temperatures for complex **2**.

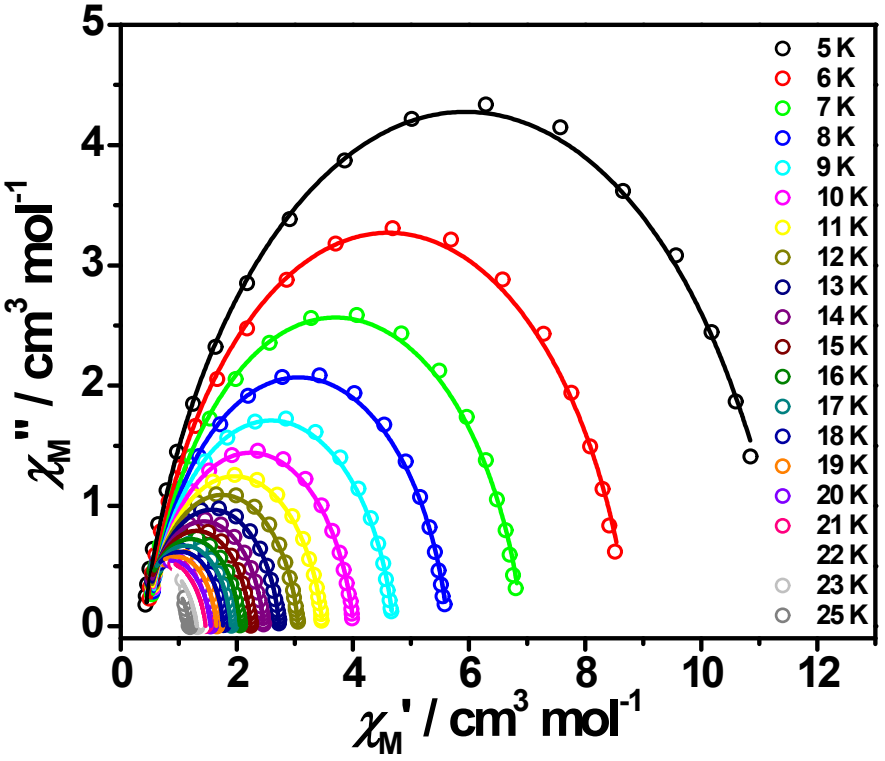

Fig. S11. Variable temperature Cole-Cole plots of complex **3** under zero dc field (1-999 Hz, by MPMS Squid VSM). Fitted parameters are compiled in supplementary Table S5.

Table S5. Analysis of Cole-Cole plot of complex **3** under zero dc field.

T	χ_S	χ_t	τ	α	*R*
5 K	0.388788	0.114834E+02	0.178714E-01	0.156962	0.890101E-01
6 K	0.456164	0.876328E+01	0.957889E-02	0.143435	0.649063E-01
7 K	0.483598	0.692302E+01	0.594537E-02	0.135735	0.364073E-01
8 K	0.490024	0.563776E+01	0.407907E-02	0.130358	0.198027E-01
9 K	0.484861	0.469954E+01	0.297237E-02	0.12447	0.111559E-01
10 K	0.469669	0.401013E+01	0.226408E-02	0.121180	0.491506E-02
11 K	0.452777	0.347530E+01	0.176277E-02	0.114134	0.255075E-02
12 K	0.434142	0.305687E+01	0.138833E-02	0.107711	0.171368E-02
13 K	0.412863	0.273123E+01	0.109983E-02	0.104510	0.138526E-02
14 K	0.397243	0.245825E+01	0.868305E-03	0.097029	0.201958E-02
15 K	0.376997	0.223736E+01	0.682924E-03	0.092330	0.198555E-02
16 K	0.356971	0.205346E+01	0.534465E-03	0.090135	0.250998E-02
17 K	0.339510	0.189643E+01	0.413786E-03	0.086216	0.283538E-02
18 K	0.310853	0.176496E+01	0.315691E-03	0.092413	0.277384E-02
19 K	0.268096	0.165001E+01	0.234137E-03	0.103480	0.287236E-02
20 K	0.227279	0.154840E+01	0.171123E-03	0.117296	0.210447E-02
21 K	0.116849	0.146092E+01	0.113925E-03	0.144329	0.155481E-02
22 K	0.261660E-10	0.138378E+01	0.731163E-04	0.169687	0.142848E-02
23 K	0.406133E-10	0.131108E+01	0.543179E-04	0.167916	0.149802E-02
25 K	0.100922E-09	0.118939E+01	0.278574E-04	0.181507	0.296969E-02

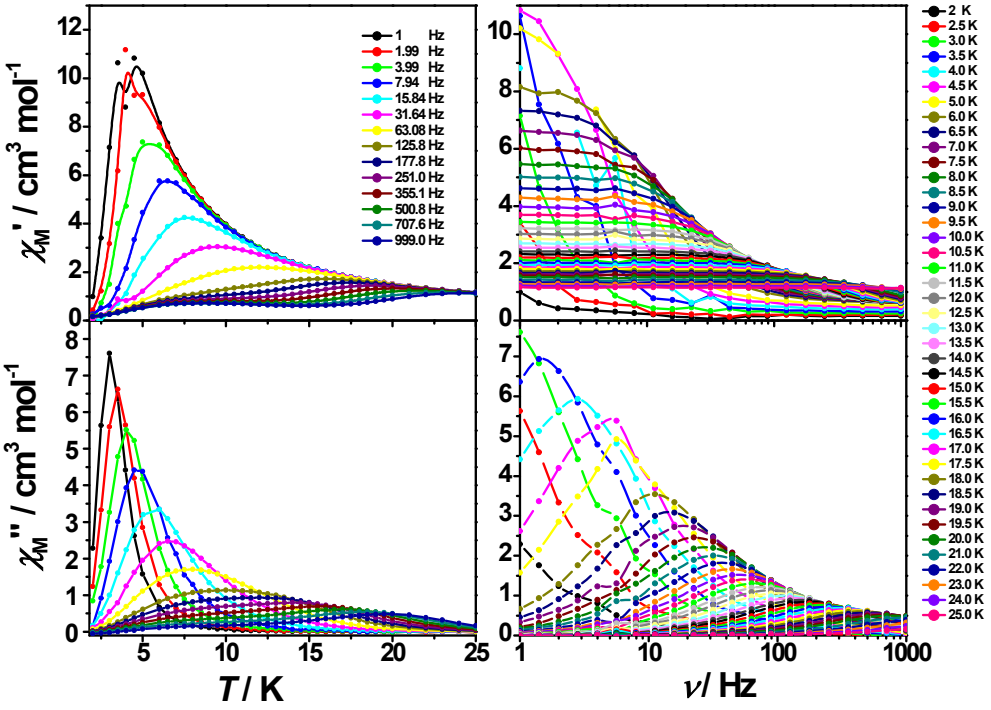

Fig. S12. Temperature (left) and frequency (right) dependence of in-phase (χ_M') and out-of- phase (χ_M'') ac susceptibilities applied 1000 Oe dc field (1-999 Hz, by MPMS Squid VSM) at indicated temperatures for complex **3**.

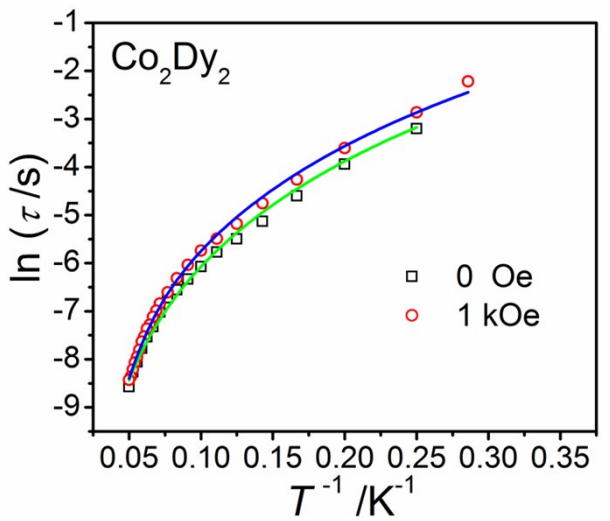

Fig. S13. Magnetization relaxation time, ln(τ), versus T^{-1} for **3**: the green solid line (under zero dc field) and the blue line (under 1000 Oe dc field) are fitted with the equation $\tau^{-1}=\tau_{QTM}^{-1}+CT^{n}+\tau_0^{-1}\exp(-U_{eff}/k_BT)$.

Table S6. Parameters used to fit the Arrhenius plots from Fig. 4 and Fig. S13 using approximations $\tau^{-1}=\tau_{QTM}^{-1}+CT^{n}+\tau_0^{-1}\exp(-U_{eff}/k_BT)$ (1)

	1@1 kOe		**3**@0 Oe		**3**@1 kOe	
	value	error	value	error	value	error
τ_{QTM}^{-1}/s^{-1}	108.36	8.9	0.001	1e-4	1e-15	-
$C/s^{-1}K^{-n}$	0.116	0.212	0.301	0.09	0.227	0.034
n	3.26	0.817	3.16	0.118	3.14	0.080
τ_0 /s	2.35e-6	6.09e-6	2.67e-6	3.9e-6	8.77e-7	1.16e-6
U /K	115	40	125	55.7	130	27.2

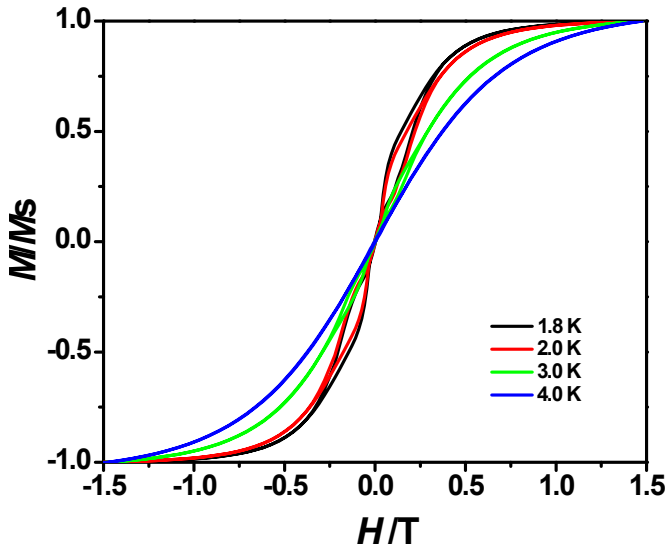

Fig. S14. Temperature-dependent magnetic hysteresis loops of **1** below 4 K.

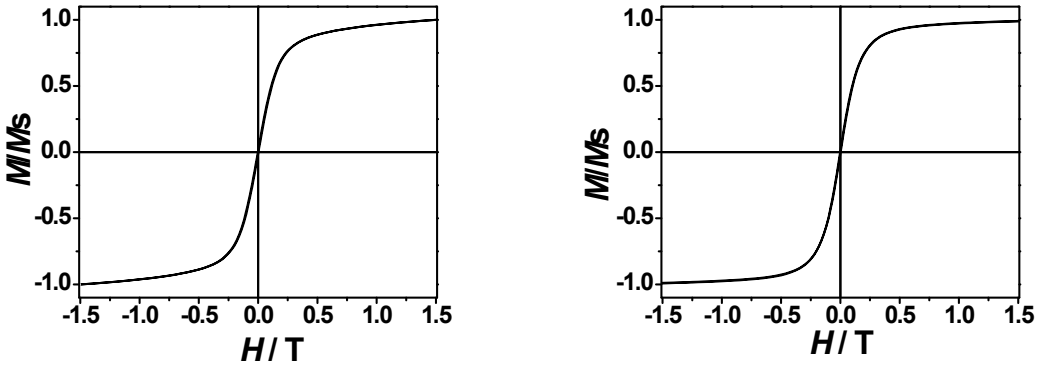

Fig. S15. Temperature-dependent magnetic hysteresis loops of **2** and **3** at 1.8 K.

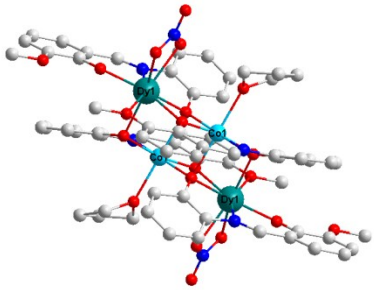

Fig. S16. Complex $[Co_2Dy_2]$ reported by Powell' group.

Table S7. Selected bond length [Å] for $[Co_2Dy_2]$ complexes reported by Powell and this paper based on Fig. S16.

	$[Co_2Dy_2]$(THF)	$[Co_2Dy_2]$(DMF)(complex **3**)
Dy1-O1	2.390	2.386
Dy1-O2	2.155	2.156
Dy1-O4	2.343	2.330
Dy1-O5	2.306	2.305
Dy1-O6	2.518	2.509
Dy1-O7	2.480	2.477
Dy1-O8	2.441	2.464
Dy1-N1	2.454	2.474
Co1-O1	2.077	2.131
Co1-O1′	2.261	2.219
Co1-O4	2.036	2.074
Co1-O5	2.038	2.028
Co1-O10[a]	2.197	2.060
Co1-N2	2.062	2.079

[a]: O10 atoms come from the solvent molecules THF and DMF, respectively.

Ab initio Calculations for 1, 2 and 3

Complete-active-space self-consistent field (CASSCF) calculations on individual lanthanide Dy^{III}, Mn^{II} (S = 5/2) and Co^{II} (S = 3/2) fragments of complexes **1**, **2** and **3** on the basis of X-ray determined geometry have been carried out with MOLCAS 7.8 program package.[1] During the calculations, the other Dy^{III}, Mn^{II} and Co^{II} ions were replaced by diamagnetic Lu^{III}, Zn^{II} and Zn^{II}, respectively. The basis sets for all atoms are atomic natural orbitals from the MOLCAS ANO-RCC library: ANO-RCC-VTZP for Dy^{III}, Mn^{II} and Co^{II} ions; VTZ for close O and N; VDZ for distant atoms. The calculations employed the second order Douglas-Kroll-Hess Hamiltonian, where scalar relativistic contractions were taken into account in the basis set and the spin-orbit couplings were handled separately in the restricted active space state interaction (RASSI-SO) procedure. For the fragment of Dy^{III}, active electrons in 7 active spaces include all f electrons (CAS(9 in 7) in the CASSCF calculation. For Mn^{II}, CAS(5 in 5) was used. For Co^{II}, CAS(7 in 10) was used. To exclude all the doubts we calculated all the roots in the active space. We have mixed the maximum number of spin-free state which was possible with our hardware (all from 21 sextets, 128 from 224 quadruplets, 130 from 490 doublets for the Dy^{III} fragment; all from 1 sextets, 24 quadruplets and 75 doublets for the Mn^{II} fragment; all from 10 quadruplets, all from 40 doublets for the Co^{II} fragment).

Table S8. Lowest Kramers doublets (cm^{-1}) and the $\boldsymbol{g}$ (g_x, g_y, g_z) tensors on the Dy^{III}, Mn^{II} and Co^{II} fragments of **1**, **2** and **3**.

1		**2**				**3**			
Dy^{III}		Dy^{III}		Mn^{II}		Dy^{III}		Co^{II}	
E	$\boldsymbol{g}$ ($\tilde{S}$ = 1/2)	E	$\boldsymbol{g}$ ($\tilde{S}$ = 1/2)	E	$\boldsymbol{g}$ ($\tilde{S}$ = 5/2)	E	$\boldsymbol{g}$ ($\tilde{S}$ = 1/2)	E	$\boldsymbol{g}$ ($\tilde{S}$ = 1/2)
0.0	0.006 0.008 19.705	0.0	0.006 0.008 19.696	0.0	2.002 2.002 2.002	0.0	0.004 0.006 19.686	0.0	1.600 2.333 7.599
229.1	0.084 0.133 16.873	202.4	0.307 0.477 16.689	0.7		206.6	0.462 1.146 16.237	140.0	2.226 2.394 5.344
384.0	2.231 3.847 14.420	292.0	0.960 1.390 17.962	1.8		266.9	0.003 1.293 17.712	827.6	0.987 3.217 5.560
444.4	8.570 5.024 1.311	374.8	0.910 3.590 11.516			379.2	0.973 4.398 11.611		
521.9	1.615 3.224 16.204	422.9	2.594 3.009 15.748			402.5	0.139 5.183 10.775		
564.3	2.344 3.667 11.590	488.2	2.072 3.727 12.734			486.3	2.829 4.801 10.896		
637.4	0.855 1.271 16.278	551.5	0.674 0.953 16.543			559.8	1.145 1.639 15.810		

714.9	0.070 0.104 19.102	663.5	0.065 0.274 18.896			633.3	0.267 0.342 19.443		

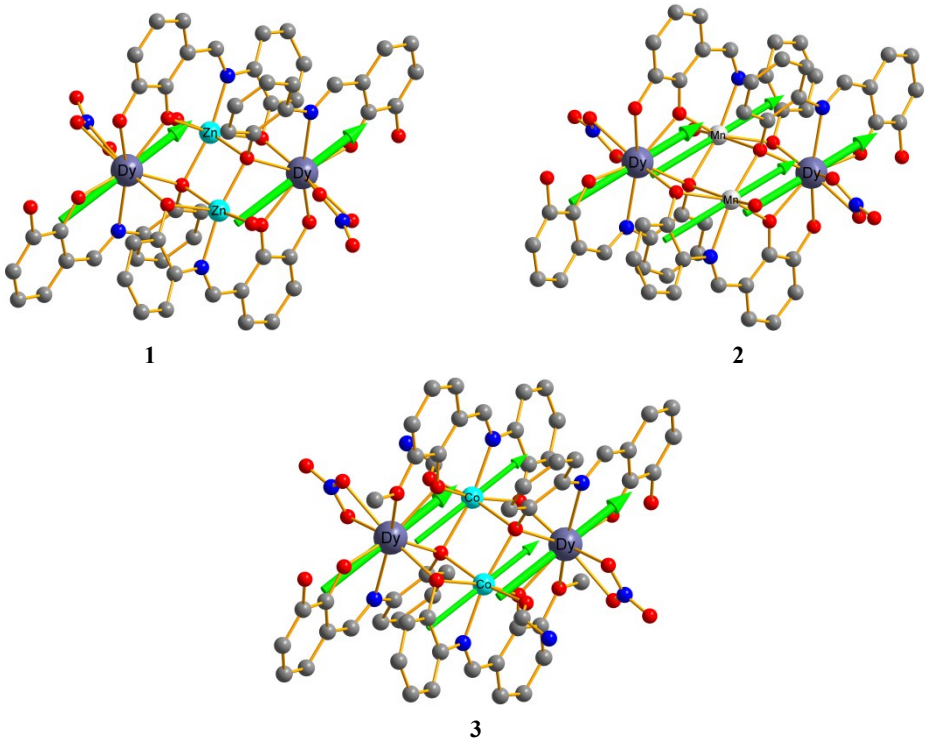

Fig. S17. Orientations of the local main magnetic axes of the ground doublets on magnetic center ions of **1**, **2** and **3**.

Fitting the exchange interaction in four complexes using Lines model based on CASSCF results

To fit the exchange interactions in four complexes, we took two steps to obtain them. Firstly, we calculated the mononuclear fragments using CASSCF to obtain the corresponding magnetic properties (see the first part). And then, the exchange interaction between the magnetic centers is considered within the Lines model,[12] while the account of the dipole-dipole magnetic coupling is treated exactly. The Lines model is effective and has been successfully used widely in the research field of 3d-4f single-molecule magnets.[13]

For complex **1**, the exchange Hamiltonian is:

$$\hat{H}_{exch} = -J_{Dy-Dy}^{total}\hat{S}_{Dy_1}\hat{S}_{Dy_2} \quad \text{(S1)}$$

For **2**, it is:

$$\hat{H}_{exch} = -J_{Dy-Mn}^{total}(\hat{S}_{Dy_1}\hat{S}_{Mn_1} + \hat{S}_{Dy_1}\hat{S}_{Mn_2} + \hat{S}_{Dy_2}\hat{S}_{Mn_1} + \hat{S}_{Dy_2}\hat{S}_{Mn_2}) - J_{Mn-Mn}^{total}\hat{S}_{Mn_1}\hat{S}_{Mn_2} - J_{Dy-Dy}^{total}\hat{S}_{Dy_1}\hat{S}_{Dy_2} \text{(S2)}$$

For **3**, it is:

$$\hat{H}_{exch} = -J_{Dy-Co}^{total}(\hat{S}_{Dy_1}\hat{S}_{Co_1} + \hat{S}_{Dy_1}\hat{S}_{Co_2} + \hat{S}_{Dy_2}\hat{S}_{Co_1} + \hat{S}_{Dy_2}\hat{S}_{Co_2}) - J_{Co-Co}^{total}\hat{S}_{Co_1}\hat{S}_{Co_2} - J_{Dy-Dy}^{total}\hat{S}_{Dy_1}\hat{S}_{Dy_2} \text{ (S3)}$$

The J_{Dy-Mn}^{total}, J_{Mn-Mn}^{total}, J_{Dy-Co}^{total} and J_{Dy-Dy}^{total} are parameters of the total magnetic interaction (J^{total} =

$J^{dipolar} + J^{exchange}$) between magnetic center ions. The $\tilde{S}_{Dy} = 1/2$ and $\tilde{S}_{Co} = 1/2$ is the ground pseudospin on the Dy and Co site, respectively, and the $\tilde{S}_{Mn} = 5/2$ is the pseudospin of the Mn site. The dipolar magnetic coupling can be calculated exactly, while the exchange coupling constants were fitted through comparison of the computed and measured magnetic susceptibility and molar magnetization using the POLY_ANISO program.[14]

Table S9. Calculated energies (cm^{-1}), the corresponding tunneling gaps (cm^{-1}) and the g_z values of the low-lying exchange doublet states of complexes **1**, **2** and **3**.

1			**2**			**3**		
E	Δ_{tun}	g_z	E	Δ_{tun}	g_z	E	Δ_{tun}	g_z
0.00	1.87E-07	39.410	0.00	8.32E-08	55.725	0.00	9.48E-10	52.082
0.40	1.46E-07	0.000	0.56	1.44E-07	53.701	8.74	4.20E-07	0.000
			0.79	1.32E-08	52.564	8.91	5.05E-07	0.000
			1.05	2.53E-08	51.158	10.22	1.01E-05	0.000
			1.19	9.27E-08	54.741	10.30	2.0E-06	39.333
			1.59	1.12E-07	44.400	11.11	2.9E-07	39.524
			1.63	2.42E-08	50.197	13.54	1.1E-07	0.000
			2.11	1.14E-07	47.866	15.74	3.0E-06	29.322
			2.13	1.07E-07	50.839			
			2.47	3.86E-07	39.902			
			2.81	9.76E-08	43.428			
			3.15	4.36E-08	46.232			
			3.33	6.88E-08	46.233			
			3.53	3.21E-07	41.472			
			3.73	8.71E-07	38.571			
			3.76	2.84E-07	40.439			
			4.72	3.71E-07	0.103			
			4.76	6.46E-06	0.102			
			4.76	5.61E-06	38.927			
			4.83	4.33E-07	37.913			
			5.02	6.47E-07	38.957			
			5.12	9.70E-06	39.187			
			5.15	2.21E-06	0.008			
			5.20	5.58E-06	35.370			
			5.30	3.22E-07	41.448			
			5.31	2.81E-07	0.015			
			5.42	5.13E-07				
			5.74	3.43E-07				
			5.90	2.13E-07				
			6.03	5.50E-08				

			6.06	3.01E-07				
			6.18	1.32E-06				
			6.24	2.22E-07				
			6.35	2.04E-06				
			6.53	5.53E-08				
			6.62	4.04E-07				
			6.72	3.17E-07				
			6.80	2.57E-07				
			6.92	3.42E-07				
			6.97	4.24E-07				
			7.09	4.98E-07				
			7.10	3.58E-07				
			7.15	2.22E-09				
			7.23	6.62E-08				
			7.36	5.34E-07				
			7.44	7.55E-07				
			7.46	4.97E-07				
			7.51	1.00E-07				
			7.56	1.22E-07				
			7.68	5.04E-07				
			7.72	1.65E-07				
			7.74	1.22E-06				
			7.76	1.07E-06				
			7.81	4.58E-07				
			8.17	4.05E-07				
			8.18	5.42E-07				
			8.24	1.62E-07				
			8.42	4.84E-07				
			8.46	2.07E-07				
			8.60	2.86E-07				
			8.73	3.68E-07				
			8.95	1.53E-07				
			8.97	2.46E-07				
			9.01	3.17E-07				
			9.15	3.06E-07				
			9.60	7.97E-08				
			9.69	1.35E-07				
			9.85	4.07E-08				
			10.49	1.32E-08				
			10.76	1.57E-08				
			11.29	8.29E-10				

			12.30	3.69E-10				

Table S10. Parameters used to fit the Arrhenius plots from Fig. 6 using approximations $\tau^{-1}=\tau_{QTM}^{-1}+CT^{n}$ (Eq. 2).

	1@0 Oe		**1**@1 kOe		**3**@0 Oe		**3**@1 kOe	
	value	error	value	error	value	error	value	error
τ_{QTM}^{-1}/s^{-1}	144.28	15.979	0	46.6	50	0	0	0
$C/s^{-1}K^{-n}$	0.00399	0.00125	0.00122	7.8e-4	0.01	0.0039	0.005	0.0015
n	4.56	0.10	4.799	0.198	4.37	0.1	4.54	0.089

References:

(1) Karlstrom, G.; Lindh, R.; Malmqvist, P. A.; Roos, B. O.; Ryde, U.; Veryazov, V.; Widmark, P. O.; Cossi, M.; Schimmelpfennig,B.; Neogrady, P.; Seijo, L. MOLCAS: a Program Package for Computational Chemistry. *Comput. Mater. Sci*. **2003**, *28*, 222-239.

(2) Neese, F. ORCA–*an ab initio, density functional and semiempirical program package*, version 2.9.1; Max-Planck institute for bioinorganic chemistry: Mülheim an der Ruhr, Germany, 2012.

(3) Becke, A. D. *J. Chem. Phys*. **1993**, *98*, 5648-5652.

(4) Becke, A. D. *Phys. Rev. A*. **1988**, *38*, 3098-3100.

(5) Lee, C.; Yang, W.; Parr R. G., *Phys. Rev. B*. **1988**, *37*, 785-789.

(6) Schäfer, A.; Horn, H.; Ahlrichs, R. *J.Chem. Phys*. **1992**, *97*, 2571-2577.

(7) Schäfer, A.; Huber, C.; Ahlrichs, R. *J. Chem. Phys.* **1994**, *100*, 5829-5835.

(8) Vieru, V.; Ungur, L.; Chibotaru, L. F. *J. Phys. Chem. Lett*. **2013**, *4*, 3565-3569.

(9) Noodleman, L. *J. Chem. Phys*. **1981**, *74*, 5737-5743.

(10) Noodleman, L.; Baerends, E. J. *J. Am. Chem. Soc.* **1984**, *106*, 2316-2327.

(11) Noodleman, L.; Case, D. A. *Adv. Inorg. Chem*. 1992, *38*, 423-458.

(12) Lines, M. E. *J. Chem. Phy*. **1971**, *55*, 2977-2984.

(13) (a) Mondal, K. C.; Sundt, A.; Lan, Y.; Kostakis, G. E.; Waldmann, O.; Ungur, L.; Chibotaru, L. F.; Anson, C. E.; Powell, A. K. *Angew. Chem. Int. Ed.* **2012**, *51*, 7550-7554;. (b) Langley, S. K.; Wielechowski, D. P.; Vieru, V.; Chilton, N. F.; Moubaraki, B.; Abrahams, B. F.; Chibotaru, L. F.; Murray, K. S. *Angew. Chem. Int. Ed.* **2013**, *52*, 12014-12019;

(14) (a) Chibotaru, L. F.; Ungur, L.; Soncini, A. *Angew. Chem. Int. Ed.* **2008**, *47*, 4126-4129. (b) Ungur, L.; Van W.; Heuvel, d.; Chibotaru, L. F. *New J. Chem.* **2009**, *33*, 1224-1230. (c) Chibotaru, L. F.; Ungur, L.; Aronica, Ch.; Elmoll, H.; Pilet, G.; Luneau, D. *J. Am. Chem. Soc.* **2008**, *130* , 12445-12455.;